Atmospheric Environment 44 (2010) 1970–1979

Contents lists available at ScienceDirect

Atmospheric Environment

journal homepage: www.elsevier.com/locate/atmosenv

Organonitrate group concentrations in submicron particles with high nitrate and organic fractions in coastal southern California

Douglas A. Day [a], Shang Liu [a], Lynn M. Russell [a,*], Paul J. Ziemann [b]

[a] Scripps Institution of Oceanography, University of California, San Diego, 9500 Gilman Drive, Mail Code 0221, La Jolla, CA 92093-0221, USA
[b] Air Pollution Research Center and Department of Environmental Sciences, University of California, Riverside, CA 92521, USA

ARTICLE INFO

Article history:
Received 14 January 2010
Received in revised form
26 February 2010
Accepted 26 February 2010

Keywords:
Organonitrate
Organic nitrates
Aerosol
FTIR
PMF

ABSTRACT

During wintertime measurements in coastal southern California, organonitrate groups accounted for up to 10% of organic mass (OM) in submicron particles. In this study, we report the calibrated absorptivity, the uncertainties in the calibrations, the detection limits for 12 and 24 h ambient sampling, and the multipeak retrieval algorithm for the method developed. Organonitrate groups were observed when both submicron particle-phase nitrate and OM concentrations exceeded 1 μg m^{-3}. These high concentrations were associated with a mixed urban fossil fuel combustion source type that had potential source regions near Riverside and the South Coast Air Basin. The high frequency of these organonitrate observations contrasts with a number of studies of aerosol particles in other regions with more humid conditions, in which organonitrate groups were not detected and submicron sulfate concentrations exceeded those of nitrate. Our results suggest both that organonitrates form and/or exist in significant concentrations during polluted urban conditions and that their lifetime may be limited by hydrolysis in the particle phase.

1. Introduction

Organonitrate molecules (R–ONO_2) have been shown to comprise 10–20% of carbonaceous aerosol mass at urban locations, of which the organonitrate functional group accounts for 5–10% of OM (O'Brien et al., 1975; Mylonas et al., 1991; Laurent and Allen, 2004). Organonitrates typically have been observed to have maximum loadings in submicron-sized particles (Mylonas et al., 1991; Garnes and Allen, 2002; Laurent and Allen, 2004). Analytical techniques employed in field studies include separation and quantification of individual organic molecules by gas chromatography mass spectrometry (GCMS) after extraction from filters and measurements of relative abundance from the spectroscopic signatures of Fourier Transform Infrared (FTIR) analysis. Recently, aerosol mass spectrometry has also been investigated as a technique to measure particulate organonitrate compounds, resulting in estimates of 0.8–1.6 μg m^{-3} (10–19% of OM) or 0.2–0.5 μg m^{-3} of organonitrate functional groups during the Study of Organic Aerosols at Riverside (SOAR) campaign (Farmer et al., 2010). In another study, Bruns et al. (2010) calculated that a ratio of at least 0.15 for the organic-to-inorganic nitrate ratio contained in aerosol is required to indicate the presence of organonitrates using an Aerosol Mass Spectrometer (AMS) and utilizing the differences in mass fragmentation patterns for ionic and covalently bound nitrate groups.

Organonitrates are formed in polluted air during the day through association reactions of NO with organic peroxy radicals (formed from VOCs via reactions initiated by OH radicals or O_3) and at night through NO_3 radical-initiated reactions of alkenes (Roberts, 1990; Atkinson, 1997; Atkinson and Arey, 2003; Gong et al., 2005; Ng et al., 2008; Fry et al., 2009; Lim and Ziemann, 2009; Matsunaga and Ziemann, 2009). Oxidation of alkanes, alkenes, and aromatics (the major atmospheric VOCs) leads to a variety of organonitrate products that are mostly multifunctional. Depending on the VOC and reaction conditions, these products can include hydroxynitrates, dihydroxynitrates, carbonylnitrates, and hydroperoxynitrates, as well as monofunctional alkyl nitrates. Studies indicate that the molar yields of first-generation high molecular weight organonitrates that can potentially form secondary organic aerosol (SOA) can approach ~40–60% for both OH and NO_3 radical reactions (Atkinson, 1997; Atkinson and Arey, 2003; Fry et al., 2009; Matsunaga and Ziemann, 2009). Alkyl nitrates, which are the most volatile organonitrates, are predicted to exist predominantly in the particle phase when carbon numbers are larger than ~C_{20} (Lim and Ziemann, 2009), but this approximate carbon number threshold will be much lower for multifunctional organonitrates.

* Corresponding author. Tel.: +1 858 534 4852; fax: +1 858 534 4851.
E-mail addresses: daday@ucsd.edu (D.A. Day), shl014@ucsd.edu (S. Liu), lmrussell@ucsd.edu (L.M. Russell), paul.ziemann@ucr.edu (P.J. Ziemann).

1352-2310/$ – see front matter © 2010 Elsevier Ltd. All rights reserved.
doi:10.1016/j.atmosenv.2010.02.045

Improved quantification of organonitrate groups in additional ambient conditions may allow for a more complete budget of organic particle mass and may provide insight into mechanisms responsible for SOA formation and sources of other functional groups. In this work, we extend the FTIR-based identification of organonitrate groups using a calibration to two laboratory standards: 2-ethylhexyl nitrate and organonitrate product mixtures formed in smog chamber reactions. The quantification of ambient organonitrate group concentrations from this technique provides further evidence of the atmospheric emission sources and ambient conditions that lead to organonitrate formation.

2. Methods

2.1. Sample collection and analysis

Measurements were made on submicron particles collected nearly continuously at the Scripps Institution of Oceanography (SIO) Pier (32°52′N, 117°15′W) from 23 February 2009 to 30 March 2009. Aerosol particles were sampled from a common inlet located 4 m above the pier (15 m above sea level) at 16.7 standard L min^{-1}. Sample air passed through a PM1 cyclone to select for submicron particles. The sample flow was split, and aerosol particles were collected on two sets of duplicate 37 mm diameter Teflon filters for quantification of organic functional groups by FTIR spectroscopy. Particles were collected continuously on one filter set for 12-h duration, with duplicate filters run in parallel for 24-h samples. 24-h samples were collected from 7 am (local, PST) to 7 am the following morning; 12-h samples typically spanned the 12-h periods from 7 am to 7 pm ("daytime") and 7 pm to 7 am ("nighttime"). Resulting total flow volumes for short and long filters were approximately 6 and 12 m^3, respectively. A smaller flow (0.07 L min^{-1}) from the same inlet was sampled by a Quadrupole AMS for quantification of size-resolved inorganic and organic mass fragments in non-refractory submicron particles.

FTIR spectroscopy was used to quantify organic functional group concentrations for the particles collected on each Teflon filter. Detailed descriptions of the method, cleanroom conditions, and standard compound calibrations for the Bruker Tensor 27 spectrometer with DTGS detector can be found in Gilardoni et al. (2007), based on similar techniques calibrated for a different spectrometer by Maria et al. (2002, 2003). Revisions to those methods include use of an automated algorithm for baselining, peak fitting, and integration, as well as additional calibrations of primary amine and carboxylic acid functional groups (Liu et al., 2009; Russell et al., 2009). The organic functional groups typically quantified include saturated aliphatic (hereafter alkane [CH]) groups, alcohol [COH] groups (including polyols and other organic hydroxyl-containing compounds), carboxylic acid [COOH] groups, non-acidic carbonyl [CO] groups, primary amine [CNH_2] groups, and organosulfate [$COSO_3$] groups; unsaturated aliphatic (hereafter alkene [CH]) groups and aromatic [CH] groups were below detection limit for all samples, with each of these two functional groups accounting for at most 3% of OM. The spectra were analyzed for evidence of organosulfate groups at 876 cm^{-1}, but detectable peaks were identified in only one sample and are excluded from this analysis. The mass associated with each mole of absorbing bonds in the identified functional group is: alkane group (7), alcohol group (23), carboxylic acid group (45), non-acid carbonyl group (28), amine group (11), organosulfate group (102), alkene group (13), aromatic group (13), and organonitrate group (68). Note that for alkane, alcohol, primary amine, and organosulfate groups, which share their C atom with another group, half of the C atom mass is assigned to each group. Identification and quantification of organonitrates are discussed in Sect. 2.2.

The AMS (Aerodyne, Billerica, MA) was used to measure mass spectra of non-refractory organic and inorganic components of submicron particles, as discussed by Jayne et al. (2000), Jimenez et al. (2003), and Allan et al. (2004). In this instrument, ambient aerosol enters through a 100 μm orifice resulting in reduced pressure (~1.2 torr) and is subsequently focused into a narrow beam (<1 mm diameter) with an aerodynamic lens. Transmission efficiency is expected to be near 100% for 60–600 nm and then decrease to about zero at ~30 nm and ~1.5 μm (Jayne et al., 2000; Jimenez et al., 2003; Zhang et al., 2004). Particles are vaporized by impaction on a ceramic heater maintained at 600 °C. The vaporization source is coupled to an electron impact ionizer (70 eV) at the entrance to a quadrupole mass spectrometer. Particle size is measured from the time-of-flight between a chopper that modulates transmission of discrete aerosol packets and chemical detection at the mass spectrometer.

During this study, AMS operation was alternated between the "mass spectrum" (MS) mode and the "time-of-flight" (TOF) mode every 5 min, with 20 m/z scanned in TOF mode. The ionization efficiency was calibrated weekly using dry 350 nm ammonium nitrate particles generated with an atomizer and size-selected with a Differential Mobility Analyzer (DMA), following mass tuning and optimization of the quadrupole mass spectrometer and electron multiplier. Analysis of the AMS measurements was accomplished with small modifications to the ion fragmentation table and "batch table" based on tests outlined in Middlebrook et al. (submitted for publication). Since AMS measurements of nitrate and sulfate include both organic and inorganic nitrate and sulfate, here we refer to these components as simply nitrate (NO_3) and sulfate (SO_4) or AMS nitrate and AMS sulfate rather than exclusively as inorganic components. However, we expect that most of these components were comprised of inorganic compounds (>90%), which is apparent in comparing the organonitrate and AMS nitrate measured in this study. Concentrations were averaged to 1 h and for the time span of each filter sample collection period. Comparison of total organic mass (OM) measured by FTIR to non-refractory OM (nrOM) measured by AMS (no collection efficiency applied) yielded a slope of 0.72 with a Pearson's correlation coefficient, r, of 0.75 (as shown in Fig. 1a). All linear regressions reported in this manuscript were calculated using a reduced major axis regression, thus allowing for comparable uncertainty in both axes. Given that FTIR OM was less than AMS nrOM, that the particle mass was less than 50% ammonium sulfate (precluding its use as a surrogate for collection efficiency, as in (Quinn et al., 2006)), and that other independent chemical comparisons were not available, there was no information to justify a non-unity collection efficiency (CE). Consequently, CE = 1 is used in this analysis. Differences between these two measures of OM may result from the uncertainties related to calibrations of both techniques (±20–25%) including the uncertainty in the assignment of relative ionization efficiencies for organic AMS mass fragments (Zhang et al., 2005b) and also to the potential for underprediction of heteroatoms in both FTIR and AMS techniques (Russell, 2003; Farmer et al., 2010).

2.2. Organonitrate calibration and quantification

The most common method used to quantify particle-phase organonitrate groups is FTIR. Peaks located at 1620–1630 cm^{-1}, 1260–1280 cm^{-1}, and 855–860 cm^{-1} have typically been used for identification and quantification (Mylonas et al., 1991; Allen et al., 1994; Dekermenjian et al., 1999). Weaker absorbances at 755 cm^{-1} and 700 cm^{-1} have also been identified for some organonitrate compounds. Both water vapor and amine functional group absorbances may interfere with the 1630 cm^{-1} peak. The absorbance peak at 1280 cm^{-1} is well suited for quantification due

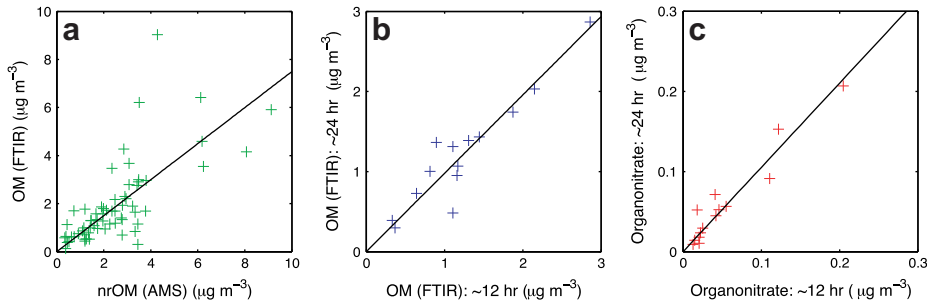

Fig. 1. Comparison of a) OM (FTIR) vs. Organics (AMS), b) OM (FTIR) ~24 h vs. ~12 h samples, and c) organonitrates (FTIR): ~24 h vs. ~12 h samples. Fitted slopes (forced through zero) are 0.72, 0.98, and 1.05 with Pearson's correlation coefficients (r) of 0.75, 0.94, and 0.96, respectively.

to its sharpness, isolation, and greater (or equal) intensity compared to other peaks.

Fig. 2 shows spectra obtained using the Bruker Tensor 27 FTIR spectrometer to analyze laboratory standards and ambient particles collected on Teflon filters. Three frequencies previously attributed to the strongest organonitrate absorption peaks are located at 1629.6, 1278.6, and 860.9 cm^{-1}. The 2-ethylhexyl nitrate (2-EHN) spectrum was produced by atomizing liquid 2-EHN (Aldrich, 97% purity) while sampling with a Teflon filter at 1 L min^{-1}. The three distinctive peaks at 1629 cm^{-1}, 1279 cm^{-1}, and 864 cm^{-1} were observed. The isobutyl nitrate (IBN) spectrum in Fig. 2b was produced by applying a drop of liquid IBN (Aldrich, 96%) directly to a Teflon filter. The samples were immediately scanned since rapid vaporization of IBN occurred, which resulted in interference at the higher frequencies due to minimal purging of the detection chamber with nitrogen gas. Three distinct organonitrate peaks were observed. The spectrum of oleic acid + NO_3 reaction products (Fig. 2c) was obtained from a filter sample collected after reacting oleic acid aerosol particles with NO_3 radicals (formed by thermal dissociation of N_2O_5) in a smog chamber at UC Riverside. The reaction products are primarily β-hydroxynitrates and β-carbonylnitrates, both of which contain a carboxylic acid group from the oleic acid (Docherty and Ziemann, 2006). The smog chamber reaction products show distinct organonitrate peaks at 1630 cm^{-1}, 1273 cm^{-1}, and 854 cm^{-1}, and a peak at 1710 cm^{-1} attributed to carbonyl groups. The spectra in Fig. 2e,f are from the products of smog chamber reactions in which 1-tetradecene and n-pentadecane were reacted separately with OH radicals in the presence of NO_x. Organonitrate products formed from the 1-tetradecene reaction are β-hydroxynitrates and dihydroxynitrates (Matsunaga and Ziemann, 2009) whereas those formed from the n-pentadecane reaction are alkyl nitrates, 1,4-hydroxynitrates, and a variety of other multifunctional mononitrates and dinitrates (Lim and Ziemann, 2009). Organonitrates in SOA filter samples collected from each reaction were quantified by spectrophotometry (Docherty and Ziemann, 2006) using 2-EHN as the calibration standard for the n-pentadecane reaction and authentic multifunctional hydroxynitrate products for the 1-tetradecene reaction (Matsunaga and Ziemann, 2009). Organonitrate peaks in these samples were observed at 1621 cm^{-1}, 1274 cm^{-1}, and 861 cm^{-1}. The locations of the peaks for the spectra from the 1-tetradecene and n-pentadecane reactions were indistinguishable. The sample collected at the Scripps pier on 1 March 2009 (Fig. 2d) shows the same three absorption peaks with different relative peak magnitudes.

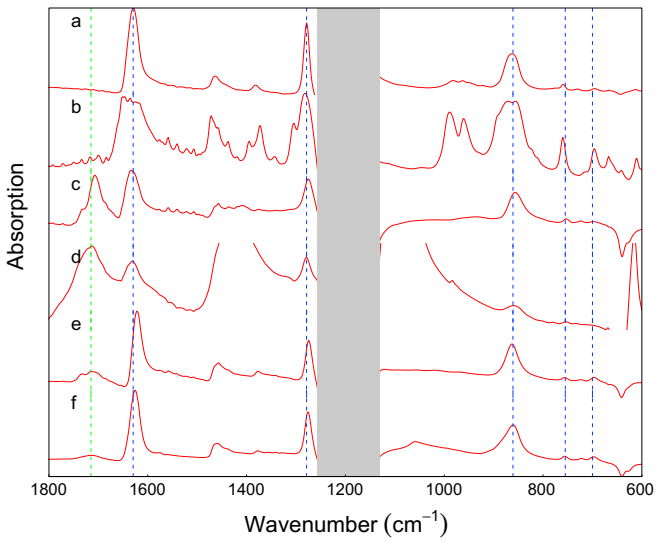

Fig. 2. FTIR spectra of a) 2-ethylhexyl nitrate, b) isobutyl nitrate, c) oleic acid + NO_3 reaction products, and d) ambient sample collected at SIO pier, e) n-pentadecane + OH/NO_x reaction products, and f) 1-tetradecene + OH/NO_x reaction products. Reactions were conducted in a smog chamber and particulate products were analyzed. Vertical lines indicate three frequencies attributed to the strongest organonitrate absorption peaks (1629.6, 1278.6, and 860.9 cm^{-1}). Frequency associated with carbonyl (1715 cm^{-1}) and two weaker organonitrate peaks (755 cm^{-1} and 700 cm^{-1}) are shown.

To quantify the absorbance associated with each peak, an automated algorithm for baselining and peak-fitting the three largest organonitrate peaks was tested using the standard and smog chamber spectra. The pre-sampling FTIR absorbance spectrum was subtracted from the post-sampling FTIR absorbance spectrum. Prior to this subtraction, both spectra were scaled by the relative Teflon absorbance to improve the comparison of the 1280 cm^{-1} peak given its proximity to the strong Teflon absorbance (1240–1250 cm^{-1}). A baseline was applied using a third-order polynomial fit to two low-absorbance regions at 700–780 cm^{-1} and 1860–2200 cm^{-1}. Fits for baselining and peak-fitting were calculated using non-linear least squares fitting. Local baselines for each of the three prominent organonitrate absorbance regions were determined using different methods. The 860 cm^{-1} peak baseline was fit with a second-order polynomial between two surrounding regions at 805–815 cm^{-1} and 925–960 cm^{-1}. The 1280 cm^{-1} peak baseline was set to a constant value determined by the local minimum between 1290 and 1320 cm^{-1}. The 1630 cm^{-1} peak was baselined using a third-order polynomial and two regions bracketing both the carbonyl and organonitrate group absorbances (1500–1550 cm^{-1} and 1850–1950 cm^{-1}). Single Gaussian functions were fit to the 860 cm^{-1} and 1280 cm^{-1} peaks and double Gaussian functions were fit to overlapping peaks at 1630 cm^{-1} (organonitrate group) and 1715 cm^{-1} (carbonyl group).

The ranges used to constrain the peak locations and widths were determined using the 2-EHN standard and smog chamber samples and implemented in the algorithm for application to ambient

spectra. Also, an additional peak was fit in the 1500–1550 region to account for primary amine absorbance, and another one was fit in the 805–960 region (constrained to 876 cm^{-1}) to account for any organosulfate absorbance that might bias the organonitrate peak quantification at that frequency. Table 1 summarizes the results of the fitting algorithm for the standards, smog chamber, and ambient sample spectra.

Absorptivities for each of the three organonitrate peaks were determined by a calibration curve using a range of mass loadings of 2-EHN. Samples were weighed before and after FTIR scanning to quantify evaporation during analysis. Fig. 3 shows the fitted peak areas as a function of organonitrate group mass loading. Error bars on the *x*-axis span the range of mass observed before and after each scan. Fits of the integrated peak area of the absorbance to the molar amount of organonitrate groups in the 2-EHN samples yielded average absorptivities of 13.3 ± 2.7, 6.5 ± 1.4, and 8.8 ± 1.7 cm^{-1} μmol^{-1} for the 1630 cm^{-1}, 1280 cm^{-1}, and 860 cm^{-1} peaks, respectively. For the smog chamber samples, the absorptivity at 1630 and 1280 cm^{-1} are lower by 20% and 60%, respectively, and at 860 cm^{-1} the absorptivity is greater by 10%.

We use the 860 cm^{-1} peak for quantification of organonitrate functional groups for ambient samples, since the absorptivity at this peak is similar between both the 2-EHN and the smog chamber samples. This choice also avoids the uncertainty resulting from interference of the amine absorbance near 1630 cm^{-1} and the Teflon absorbance near 1280 cm^{-1}. Detection limits were calculated to be the peak area that exceeds the peak areas of the blank filters collected as back-up filters for each sample at a 95% confidence level. For 12-h and 24-h samples, that detection limit corresponded to 0.01 and 0.005 $\mu g\ m^{-3}$, respectively. The uncertainty for ambient organonitrate concentrations presented here is the greater of half of this detection limit or the uncertainty in the measured absorptivity (±25%). Reanalysis of eleven samples for organonitrate concentrations after 11 months of storage yielded concentrations at 70% of the initial values indicating that large evaporative or chemical losses between sampling and analysis are unlikely. Other functional groups did not show significant decreases following reanalysis. Typical sample histories included one day of equilibration at 55% RH and 20 °C in the cleanroom environment prior to analysis, followed by storage at −4 °C.

3. Results

Fig. 4 and Table 2 show the variation and averages of the FTIR and AMS measurements of submicron particle components during the campaign. OM concentrations were 1.6 ± 1.4 $\mu g\ m^{-3}$, with daytime averages slightly higher and more variable than during nighttime. Alkane functional groups comprised the largest fraction of OM throughout most of the campaign, on average 40% (0.72 ± 0.85 $\mu g\ m^{-3}$). Alcohol and carboxylic acid functional groups represented the other major contributions to OM at 25% of OM each, with averages and standard deviations of 0.29 ± 0.19 $\mu g\ m^{-3}$ and 0.40 ± 0.39 $\mu g\ m^{-3}$, respectively. On average, amine, organonitrate, and non-acid carbonyl functional groups (primarily ketones, aldehydes, and esters) each comprised <10% of OM. Organonitrate groups were observed to vary over a large range of concentrations from 0.008 to 0.43 $\mu g\ m^{-3}$, or 0.8 to 9% of OM. Oxygen-to-carbon ratios were on average 0.57 ± 0.18, showing moderately higher ratios during nighttime. Concentrations of alkane and carboxylic acid functional groups showed slightly larger concentrations during daytime, while alcohol functional groups were lower. Fig. 4 (top) shows the time series of the organic functional groups (short, ~12-h samples only), demonstrating the large variability in OM, which ranged from 0.1 to 9 $\mu g\ m^{-3}$. The concentrations tended to vary on 3–5 day (synoptic) timescales with relatively small differences between daytime and nighttime samples.

Inorganic and organic compounds measured by AMS are summarized in Table 2. On average, nrOM constituted nearly half of the total AMS non-refractory submicron particle mass (41 ± 14%, 2.1 ± 1.7 $\mu g\ m^{-3}$). Sulfate was the second largest contribution at 37 ± 19% (1.5 ± 0.8 $\mu g\ m^{-3}$). Nitrate and ammonium were comparable, representing on average 11–12% of the AMS mass (0.69 ± 1.0 $\mu g\ m^{-3}$ and 0.60 ± 0.43 $\mu g\ m^{-3}$). Nitrate was quite variable, however, with concentrations varying by a factor of 100, corresponding to relative contributions of 1.5% to more than 30%. On average, for the 36-day campaign, ammonium, sulfate, nitrate, and nrOM showed no significant differences between nighttime and daytime concentrations or mass fractions. The time series of these components show changes on 3–5 day timescales, largely tracking changes in the functional group composition.

In order to identify the types of sources that contributed to these changing organic mixtures, we used positive matrix factorization (PMF) of both the FTIR mass-weighted spectra (e.g. Russell et al., 2009) and the AMS mass spectra (e.g. Ulbrich et al., 2009) to separate source contributions to the particle components (Alfarra et al., 2004). Different FPEAK rotation parameter values (−0.2, 0, 0.2, and 0.4) resulted in the same factors; therefore, FPEAK = 0 was used to represent the solution for both analyses.

3.1. FTIR PMF analysis

For the FTIR spectra from 1600 to 3600 cm^{-1}, two- to six-factor solutions with FPEAK were investigated. The five-factor solution

Table 1
Summary of peak-fitting results and absorptivity quantification. Means and standard deviations (parenthesis) for each sample set are shown for three peak locations (cm^{-1}), peak widths (cm^{-1}; $\sigma 2^{0.5}$), and relative absorptivities.

	Isobutyl nitrate (IBN)	2-Ethylhexyl nitrate (EHN)	Oleic acid + NO_3	1-Tetradecene or *n*-pentadecane (+OH/NO_x)	Pier Winter 2009
Location 1	1630.2 (2.3)	1629.0 (1.5)	1629.6 (–)	1621.3 (2.0)	1634.5 (1.0)
Width 1	43.4 (0.3)	17.8 (2.8)	22.6 (–)	14.6 (1.2)	18.7 (3.3)
Location 2	1283.9 (0.6)	1278.5 (0.5)	1273.3 (–)	1274.2 (0.7)	1280.2 (2.1)
Width 2	20.6 (0.3)	9.9 (2.2)	15.6 (–)	8.8 (0.5)	10.6 (2.5)
Location 3	864.7 (0.1)	863.8 (1.1)	854.3 (–)	861.0 (2.9)	854.1 (0.1)
Width 3	35.0 (0.3)	19.4 (0.8)	21.3 (–)	25.3 (5.1)	22.2 (7.2)
Area 1:Area 2	2.05 (0.04)	2.13 (0.21)	2.16 (–)	2.6 (0.28)	1.93 (0.98)
Area 3:Area 2	1.71 (0.11)	1.22 (0.08)	1.21 (–)	2.2 (0.50)	0.91 (0.52)
Sample size	2	12	1	6	114
Absorptivity 1 (area μmol^{-1})	–	13.3 (2.7)	–	10.9 (2.5)	–
Absorptivity 2 (area μmol^{-1})	–	6.5 (1.4)	–	4.1 (0.9)	–
Absorptivity 3 (area μmol^{-1})	–	8.8 (1.7)	–	9.8 (0.8)	–

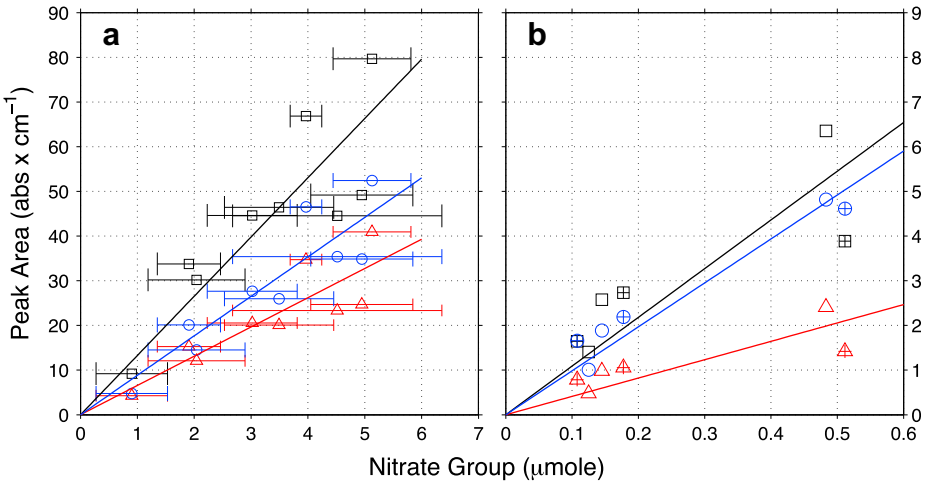

Fig. 3. a) 2-Ethyl-hexyl nitrate absorptivity calibration: FTIR peak area (absorbance cm^{-1}) vs. organic nitrate functional group applied to filter. Calculated slopes provide absorptivity used to calculate organic nitrate filter loading for ambient samples. b) Absorptivity calibration for smog chamber aerosol formed from OH/NO_x reactions of 1-tetradecene or *n*-pentadecane. Fitted slopes for 2-ethyl-hexyl nitrate calibration for 1630 (squares), 1280 (triangles), and 860 (circles) peaks is 13.3, 6.5, and 8.8 with Pearson's correlation coefficients (r) of 0.85, 0.86, and 0.90, respectively. For 1-tetradecene or *n*-pentadecane products, slopes were 10.9, 4.1, and 9.8, with r values of 0.86, 0.83, and 0.97 (fits forced through zero). In panel b, 1-tetradecene samples are denoted by a "+" overlaid on the markers.

was chosen since it reproduced the measured OM best among all the solutions (with a slope of 1.05 and an $r = 0.93$) and resulted in factors with smoothly-varying FTIR spectra with spectral features similar to those reported for known organic components of the atmosphere. The five factors were divided into two groups of correlated factors, and the factors in each group have similar potential source regions. A two-factor solution was generated from recombination of factors in each group, yielding two independent factors that were identified as a Combustion Factor and a Marine Factor, due to their correlation with inorganic components (sulfate and nitrate) and potential source locations, as described below. We interpret the identification of only two factors to mean that the different types and locations of sources that influenced the organic composition during the campaign were too similar to be fully resolved with the limited number of samples and campaign duration.

Compositions and correlations of these factors are summarized in Table 2. The Combustion Factor was on average 1.4 μg m^{-3} and comprised 80% of PMF OM (on a sample-by-sample basis). The Marine Factor was smaller, averaging 0.26 μg m^{-3} and comprising the other 20% of the PMF OM. The OM reconstructed from PMF factors tracks the measured OM well and showed a large temporal variability. Fig. 4 shows the time series of the two factors identified as fractions of OM resolved by PMF. The Combustion Factor was approximately half alkane (49%, 0.69 μg m^{-3}) with carboxylic acid comprising the other dominant fraction (27%, 0.38 μg m^{-3}). Amine and alcohol functional groups were minor fractions (7% each). The Marine Factor was dominated by alcohol functional groups, which comprised 81% (0.21 μg m^{-3}) of the OM assigned to this factor, and alkane and amine groups were 6% and 13%, respectively (cf. Table 2 and Fig. 4). The chemical composition of these factors are comparable to other Combustion and Marine Factors that have been

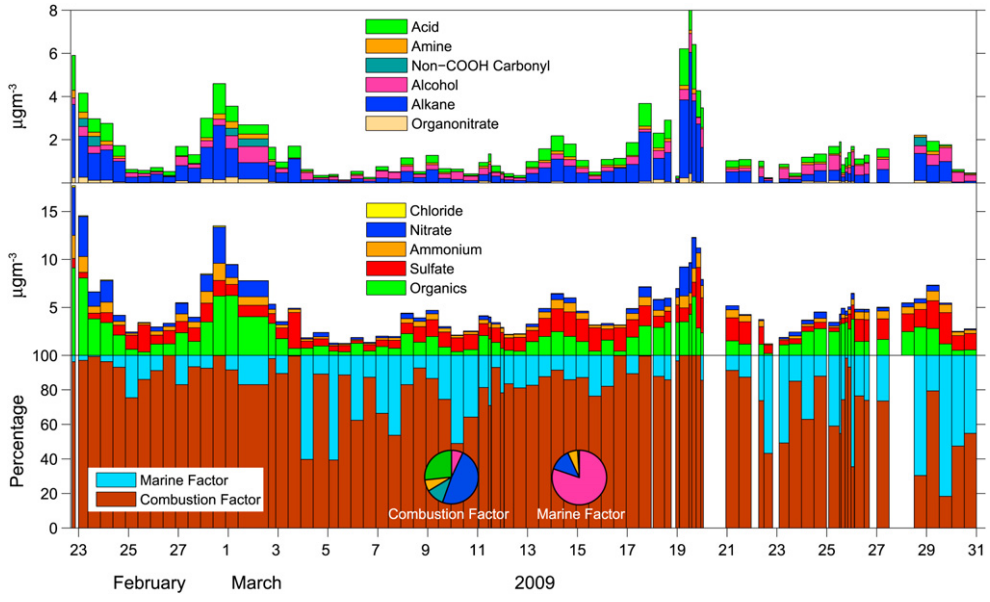

Fig. 4. (top panel) FTIR functional groups concentrations (~12-h samples), (middle panel) AMS concentrations averaged onto FTIR sample timestamp, and (bottom panel) FTIR PMF factors as a fraction of total OM resolved by PMF. Pies graphs showing the chemical composition for the PMF factors are also shown in the bottom panel (see top panel for legend).

Table 2
Summary of FTIR, AMS, and PMF results.

		Project average		Day		Night		FTIR PMF combustion factor		FTIR PMF marine factor	
		μg m^{-3}	Fraction of OM or AMS (%)	μg m^{-3}	Fraction of OM or AMS (%)	μg m^{-3}	Fraction of OM or AMS (%)	μg m^{-3}	Fraction of Factor (%)	μg m^{-3}	Fraction of OM or AMS (%)
FTIR Organic Functional Groups	OM	1.6 ± 1.4	100	1.7 ± 1.8	100	1.5 ± 1.2	100	1.40	100	0.26	100
	Alkane	0.72 ± 0.85	40 ± 12	0.88 ± 1.1	42 ± 13	0.64 ± 0.67	38 ± 11	0.69	49	0.03	13
	Alcohol	0.29 ± 0.19	25 ± 15	0.25 ± 0.17	23 ± 16	0.34 ± 0.18	29 ± 15	0.10	7	0.21	81
	Carboxylic acid	0.40 ± 0.39	24 ± 8	0.46 ± 0.51	25 ± 10	0.38 ± 0.33	24 ± 6	0.38	27	0.00	1
	Non-acid carbonyl	0.03 ± 0.10	1.5 ± 4.7	0.02 ± 0.09	1.5 ± 5.9	0.02 ± 0.08	0.5 ± 2.1	0.15	11	0.00	0
	Amine	0.08 ± 0.07	5.7 ± 2.8	0.08 ± 0.07	5.7 ± 3.3	0.08 ± 0.07	5.9 ± 2.7	0.10	7	0.02	6
	Organonitrate	0.06 ± 0.07	3.2 ± 2.0	0.05 ± 0.08	2.7 ± 1.9	0.06 ± 0.07	3.4 ± 2.3	$r = 0.70$		$r = 0.05$	
	O/C	0.57 ± 0.18	–	0.50 ± 0.18	–	0.63 ± 0.19	–	0.40		1.25	
AMS	NO_3	0.69 ± 1.0	11 ± 8	0.67 ± 1.06	10 ± 8	0.63 ± 0.84	10 ± 7	$r = 0.82$		$r = -0.09$	
	SO_4	1.5 ± 0.8	37 ± 19	1.6 ± 1.1	40 ± 22	1.5 ± 0.7	35 ± 16	$r = 0.21$		$r = 0.15$	
	NH_4^+	0.60 ± 0.43	12 ± 3	0.59 ± 0.47	11 ± 3	0.61 ± 0.36	12 ± 3	$r = 0.85$		$r = 0.04$	
	nrOM	2.1 ± 1.7	41 ± 14	2.1 ± 1.8	39 ± 17	2.1 ± 1.5	42 ± 13	$r = 0.82$		$r = 0.05$	

observed at several other locations (Bahadur et al., in press; Liu et al., 2009; Russell et al., 2009, in press; Hawkins et al., in press), where combustion factors are dominated by alkane groups with substantial acid contributions, and marine factors are dominated by hydroxyl groups (marine saccharides). The Combustion Factor showed moderate to strong correlations with all of the AMS chemical groups except sulfate, whereas the Marine Factor was not correlated with any of the measured components (listed in Table 2). Potential Source Contribution Function analysis (Sect. 4.1) showed that the Combustion Factor had sources primarily near populated continental regions (similar to OM in Fig. 5b), whereas the Marine Factor generally showed diffuse sources mostly over the ocean.

3.2. AMS PMF analysis

The input files for PMF analysis of AMS spectra were prepared using the IGOR code based on the work of Zhang et al. (2005a). The measured OM was well reproduced for all the solutions (with $r = 1$ and slope of 0.98). Small, correlated factors were generated when the number of factors was larger than three, indicating that more than enough factors were used. The factors were determined after recombination of the correlated factors among all the solutions. The 3-factor solution with the first two factors recombined was selected to represent the most likely factors.

The normalized spectrum of the first factor correlates with several OOA spectra from the AMS spectra database (Ulbrich et al., 2009).

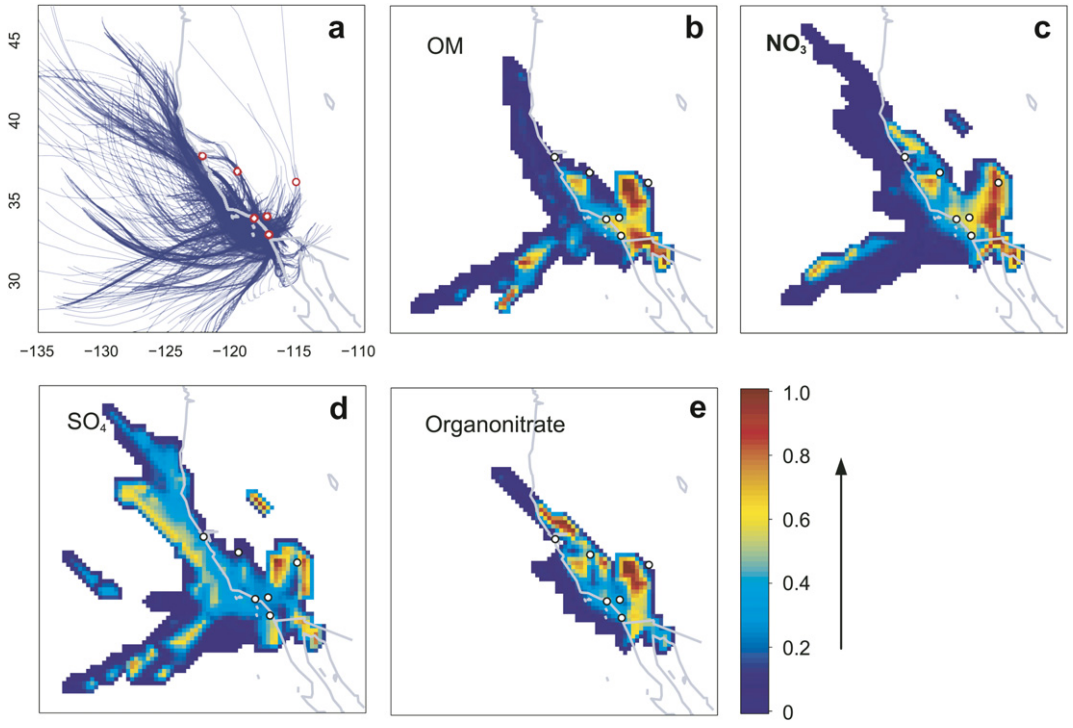

Fig. 5. a) Map showing all 1-day back trajectories (hourly) at Scripps Pier used for Potential Source Contribution Function (PSCF) analysis of February–March, 2009 measurements. PSCF images of b) FTIR OM, c) AMS nitrate, d) AMS sulfate, and e) organonitrate concentrations. Circles shown in each map (most northern three points, left to right) indicate San Francisco, Fresno, and Las Vegas and (most southern three points, starting at upper left and moving clockwise) Los Angeles/Long Beach, Riverside, and Scripps Pier. Grey lines indicate the coastline and U.S.-Mexico border. Heat map coloring represents probability of source regions for each respective compound.

For example, it correlates with the OOA factor spectrum from ambient aged combustion sources likely dominated by traffic (with $r = 0.99$ for all measured m/z values and $r = 0.98$ for $m/z > 44$ (Alfarra et al., 2004)) and with the SOA spectrum from the oxidation of laboratory-generated diesel exhaust (with $r = 0.96$ for all m/z and $r = 0.97$ for m/z greater than 44 (Sage et al., 2008)). It also correlates with the OOA spectrum from the oxidation of *m*-xylene with $r = 0.93$ for $m/z \leq 44$ and $r = 0.90$ for $m/z > 44$. This combustion-like factor also correlates with ammonium and nitrate with $r > 0.5$. Nitrate is formed from the oxidation of NO_x, which is dominated by vehicular sources. Potential Source Contribution Function (PSCF) analysis shows nitrate emissions are likely from urban sources close to or upwind of Riverside (Fig. 5). Ammonium and nitrate correlate with $r = 0.8$ and are likely from co-located sources.

The first factor was assigned as an aged Combustion Factor, due to the similarity of its spectrum to other published OOA spectra and correlation with nitrate and ammonium. It is characterized by a large m/z 44 contribution (15% of nrOM, as listed in Table 2). The m/z 43 and m/z 57 account for 6.3% and 1.5% of the factor OM, respectively. This nrOM factor has an average nrOM concentration of 1.9 μg m^{-3} and constitutes 83% of nrOM (on a sample-by-sample basis). Because of its spectral similarity to urban OOA factors and its correlation to ammonium and nitrate, this factor is likely to originate from combustion sources. The second AMS OM factor time series does not correlate with the time series of AMS-measured inorganic species. No correlation was found between the factor spectrum and spectra from the AMS database. PSCF analysis shows that increased concentration of the second factor was associated with marine trajectories. The small fraction of alkane or carboxylic acid group absorption and the low sulfate concentration associated with this factor suggests that shipping emissions is an unlikely source. Since this factor lacks similarity to AMS spectra measured for saccharide (a likely constituent of marine organic particles) reference standards (Russell et al., in press) and there were no data to show a correlation to NaCl or wind speed, we identify it only as a non-combustion factor with OM of 0.2 μg m^{-3}, accounting for 17% of the AMS nrOM.

In summary, PMF analysis of both FTIR and AMS spectra resulted in two factors, representing a combustion source and another source, with the Combustion Factor accounting for 80–83% of the FTIR OM. Both combustion factors correlate with ammonium, nitrate, and m/z 44 concentrations. The time series of the FTIR- and the AMS-Combustion Factor OM concentrations correlate to each other with a similar correlation coefficient ($r = 0.73$) compared to that for measured FTIR OM and AMS nrOM ($r = 0.75$). The non-combustion factors resulting from the FTIR and AMS measurements have a weak correlation with $r = 0.4$, and the FTIR-Marine Factor is 30% larger than the AMS non-combustion factor. The AMS does not measure refractory particles, including NaCl, which may account for the weak correlation and the lower mass of the AMS non-combustion factor relative to the FTIR Marine Factor (OM on sea salt particles will be quantified by FTIR while such particles may bounce off the AMS vaporizer and not be quantified). The good agreement between the FTIR and AMS Combustion Factors shows the consistency of the two measurements and provides evidence for the robustness of the factor separation.

4. Discussion

Over the past decade, several studies of the chemical composition of fine particles have been conducted in the South Coast Air Basin, likely an important source region for the particles observed in this study. Sardar et al. (2005) discuss PM2.5 measurements made at four sites including Riverside and Long Beach during fall, winter, and summer. During winter, average mass fractions of OC, nitrate, and sulfate at the four sites fell in the ranges 30–60%, 30–50%, and 15–25% (total PM2.5 mass: 9–17 μg m^{-3}), respectively. As part of the SOAR-1 campaign conducted in Riverside during summer, Grover et al. (2008) observed PM2.5 aerosol with the average concentrations of OC, inorganic nitrate, and sulfate of 6.2, 5.7, and 4.3 μg m^{-3}, respectively. For the same study, Zhang et al. (2007) report average submicron particle mass concentrations of 19 μg m^{-3} composed of approximately 45% OM, 20% nitrate, 20% sulfate, and 15% ammonium. Their observed 40/20/20/15 split among organic/nitrate/sulfate/ammonium is similar to the 41/11/37/12 split reported for this campaign, in which the lower average nitrate/sulfate ratio (less than 1/3 rather than 1/1) may reflect the local coastal or shipping contributions. The lower mass concentrations and nitrate contributions may reflect the dilution and losses during transit from the South Coast Air Basin.

4.1. PSCF analysis

The time series of the chemical concentrations or aerosol fractions and PMF factors were paired with back trajectories to identify the most likely source regions using PSCF maps (Ashbaugh et al., 1985; Hopke et al., 1995). For the PSCF analysis of AMS concentrations and fractions, the time series were averaged hourly and paired with hourly back trajectories. 12 hourly back trajectories were associated with the 12-h FTIR filter samples. Periods for which concentrations exceeded the 65th (OM and nitrate) or 75th (sulfate and organonitrate groups) percentile concentrations were classified as high periods. To reduce the inclusion of grid cells with large uncertainties, a cumulative distribution function of trajectory passing over grid cells (56 × 69 km) was used to set a threshold of 50% so that the cells with less than 120 trajectory crossings were not considered in the PSCF calculation. In order to focus the source identification on boundary layer sources, when trajectories were higher than 1000 m above ground level, their associated receptor concentrations were not used in the PSCF analysis for those grid cells. Fig. 5a shows a composite image of all hourly back trajectories (2-day) ending at the Scripps pier at 200 m asl. A large fraction of trajectories pass over urban locations in southern California and extend as far as Las Vegas. Many of the remaining trajectories came from the Pacific Ocean or along the coastline from the northwest. Fig. 5b shows that the source regions of the FTIR OM are likely to have contributions from the South Coast Air Basin as well as the San Joaquin Valley which extend into San Bernardino and Riverside Counties, with a few trajectories showing some contribution from northeastern Baja California (between Mexicali and the Sea of Cortez). Similarly, AMS nitrate and organonitrates (Fig. 5c,e) shows sources that largely overlap these same continental regions in addition to north of the San Francisco Bay Area in Sonoma, Marin, and Contra Costa Counties. In addition, OM, AMS nitrate, and organonitrate groups (Fig. 5b,c,e) show potential sources west of Fresno in Monterey County. In contrast, the AMS sulfate concentrations (Fig. 5d) show marine sources, with their potential source regions off the coast along shipping lanes extending to north of the San Francisco Bay Area. The inland areas identified as potential sources of sulfate in San Bernardino County may be associated with diesel emissions.

4.2. Organonitrates

Fig. 5e shows the possible source regions of organonitrates. The concentrations of FTIR organonitrate groups show strong similarities to the FTIR OM source regions (Fig. 5b). This geographic coincidence is likely due to the co-location of VOC, NO_x, and SOA precursors that contribute to both the largely combustion-dominated OM and organonitrate formation. Fig. 5e also shows the

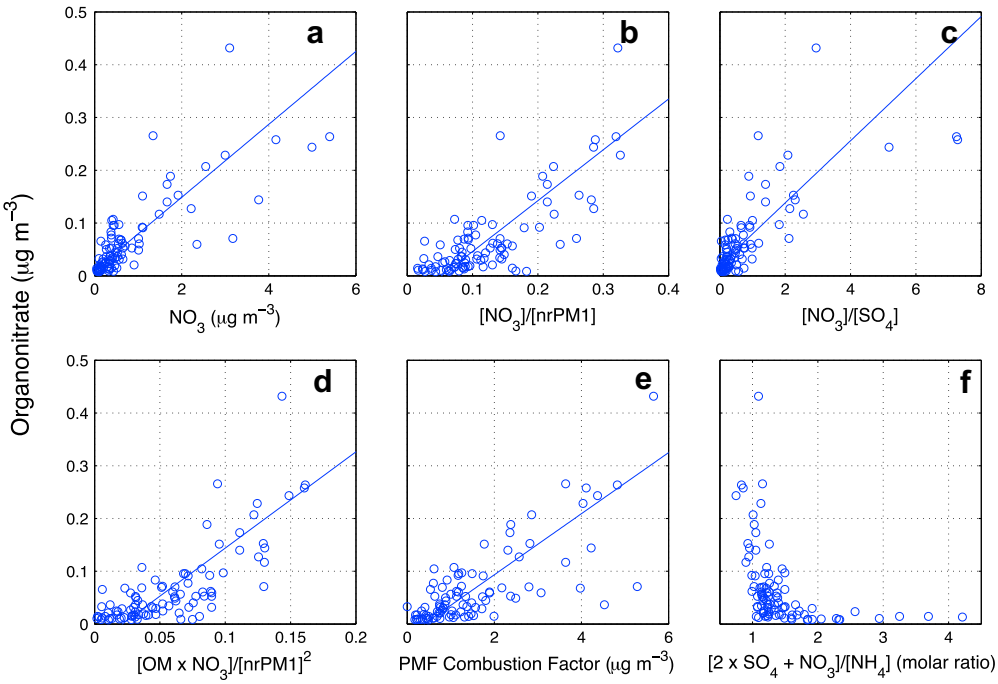

Fig. 6. Scatter plots of organonitrate concentrations vs. a) AMS nitrate, b) AMS nitrate mass fraction, c) $[NO_3]/[SO_4]$, d) $[OM \times NO_3]/[nrPM1]^2$, e) FTIR PMF Combustion Factor, and f) $[2 \times SO_4^{2-} + NO_3]/[NH_4^+]$. Fitted slopes for a–e are: 0.074, 1.0, 0.059, 1.9, and 0.058, with Pearson's correlation coefficients (r) of 0.76, 0.75, 0.72, 0.74, and 0.70, respectively.

approximate overlap of source regions for organonitrate and AMS nitrate sources. Both organonitrate groups (Fig. 5c) and AMS nitrate (Fig. 5e) indicate source regions in the vicinity of the San Francisco Bay Area. Equally notable is the absence of organonitrate groups in the marine and coastal source regions.

Fig. 6 shows a series of correlations for organonitrate groups with several submicron aerosol constituents. Organonitrate groups show a strong correlation with both AMS nitrate concentration and mass fraction ($r = 0.76$ and $r = 0.75$, respectively) suggesting that either inorganic nitrate may play a role in organonitrate formation or that the sources and conditions that favor their formation co-occur. FTIR organonitrate group concentrations also correlated with the AMS nitrate to AMS sulfate ratio with $r = 0.72$. Fig. 6d shows that the correlations of organonitrate with the product of OM/nrPM1 (total non-refractory PM1 as measured by AMS) and with the AMS nitrate fraction of non-refractory submicron mass (NO_3/nrPM1) are strong. This result suggests that conditions reflected by both higher OM and inorganic nitrate fractions in this study also favored organonitrate formation, likely due to significant organonitrate functional group production during SOA formation in high NO_x regions. Similarly, the FTIR Combustion Factor had a strong correlation with organonitrate group concentrations.

Both organonitrate and amine functional groups correlated strongly with OM ($r = 0.80$ and $r = 0.70$, respectively), and organonitrate groups showed a similar correlation with amines ($r = 0.72$), suggesting their sources may coincide in this region. Organonitrate group concentrations showed a moderate correlation with ammonium concentration ($r = 0.56$). In fact this correlation may, in part, be due to the fact that the presence of increased NH_3 will result in shifting the $NH_3(g) - HNO_3(g) - NH_4NO_3(s)$ equilibrium toward the particle phase. Often the anion – cation balance is used as an indication of the particle acidity (Quinn et al., 2006). The ratio of total [2*sulfate + nitrate]/[ammonium] was considered here as a surrogate for acidity. The relationship between organonitrate concentration and this "acidity" showed that organonitrates were only detected in significant quantities when the acidity was low (anions >75% neutralized; Fig. 6f). Given that smog chamber results have identified numerous significant gas-phase formation pathways for organonitrate compounds whereas condensed-phase pathways are not well established, we speculate that the relationship with particle phase nitrate and ammonium components suggests that acidic aqueous conditions could lead to the further reaction and removal of organonitrate groups in the particle phase. Although kinetics studies on monofunctional alkyl nitrates suggests that these pathways would be rather slow (Roberts, 1990), more recent evidence indicates that they may be significantly faster for multifunctional hydroxynitrates of the type expected to form SOA (Sato, 2008). Since our measurements are several hours downwind of the expected formation in Riverside, we expect that organonitrate groups would only remain to be measured in particles that are sufficiently dry to preclude their hydrolytic destruction. Relative humidity recorded for inland regions in Southern California such as Riverside during this study were characterized by mid-day lows of 45 ± 20% with nighttime highs of 70 ± 10% (http://www.arb.ca.gov/aqmis2/metselect.php). While these relative humidities may include deliquesced particles of a variety of composition, the lack of relative humidities above 80% reduces the likelihood of the faster chemical processing expected for liquid-phase cloud, smog, or fog conditions (Seinfeld and Pandis, 2006).

5. Conclusions

The quantification of organonitrate functional groups from calibrated FTIR absorptivities was used to show that organonitrate groups can account for almost 10% of OM in particles produced from urban combustion emissions. The presence of organonitrate groups is linked with significant organic concentrations, much of which reflects highly oxygenated compounds associated with modern fossil fuel combustion emissions. The South Coast Air Basin has been shown to be a significant source of such emissions, along with 20% or more contributions of inorganic nitrate to nrPM1.

In addition to corresponding to both high organic and high nitrate conditions, the probability of forming and/or retaining organonitrates seems to be larger when sulfate and humidity are low.

Since multifunctional organonitrate compounds have been shown to form from oxidation in the gas phase, these measurements suggest that sulfate, other acidic particle components, and the presence of high humidities may enhance the destruction of organonitrate components in the particle phase. The presence of sufficient ammonium to neutralize both nitrate and sulfate components and lower humidities may slow this reaction pathway, providing a longer lifetime of organonitrate products in these conditions.

Acknowledgments

This work was supported by NSF grants ATM-0904203, ATM-0744636, and ATM-0650061. We thank Aiko Matsunaga and Sukon Aimanant for preparing smog chamber samples at UC Riverside.

References

Alfarra, M.R., Coe, H., Allan, J.D., Bower, K.N., Boudries, H., Canagaratna, M.R., Jimenez, J.L., Jayne, J.T., Garforth, A.A., Li, S.M., Worsnop, D.R., 2004. Characterization of urban and rural organic particulate in the Lower Fraser Valley using two Aerodyne Aerosol Mass Spectrometers. Atmospheric Environment 38, 5745–5758. doi:10.1016/j.atmosenv.2004.01.054.

Allan, J.D., Delia, A.E., Coe, H., Bower, K.N., Alfarra, M.R., Jimenez, J.L., Middlebrook, A.M., Drewnick, F., Onasch, T.B., Canagaratna, M.R., Jayne, J.T., Worsnopf, D.R., 2004. A generalised method for the extraction of chemically resolved mass spectra from Aerodyne Aerosol Mass Spectrometer data. Journal of Aerosol Science 35, 909–922. doi:10.1016/j.jaerosci.2004.02.007.

Allen, D.T., Palen, E.J., Haimov, M.I., Hering, S.V., Young, J.R., 1994. Fourier transform infrared spectroscopy of aerosol collected in a low pressure impactor (LPI/FTIR): method development and field calibration. Aerosol Science and Technology 21, 325–342. doi:10.1080/02786829408959719.

Ashbaugh, L.L., Malm, W.C., Sadeh, W.Z., 1985. A residence time probability analysis of sulfur concentrations at Grand-Canyon-National-Park. Atmospheric Environment 19, 1263–1270.

Atkinson, R., 1997. Gas-phase tropospheric chemistry of volatile organic compounds: 1. Alkanes and alkenes. Journal of Physical and Chemical Reference Data 26, 215–290.

Atkinson, R., Arey, J., 2003. Atmospheric degradation of volatile organic compounds. Chemical Reviews 103, 4605–4638. doi:10.1021/cr0206420.

Bahadur, R., Uplinger, T., Russell, L.M., Sive, B.C., Cliff, S.S., Millet, D.B., Goldstein, A.H., Bates, T.S. Phenols groups in Northeastern U.S. submicron aerosol particles produced from seawater sources. Environmental Science and Technology, in press.

Bruns, A.E., Perraud, V., Zelenyuk, A., Ezell, M.J., Johnson, S.N., Yu, Y., Imre, D., Finlayson-Pitts, B.J., Alexander, M.L., 2010. Comparison of FTIR and particle mass spectrometry for the measurement of particulate organic nitrates. Environmental Science and Technology 43, 1056–1061.

Dekermenjian, M., Allen, D.T., Atkinson, R., Arey, J., 1999. FTIR analysis of aerosol formed in the photooxidation of naphthalene. Aerosol Science and Technology 30, 273–279.

Docherty, K.S., Ziemann, P.J., 2006. Reaction of oleic acid particles with NO_3 radicals: products, mechanism, and implications for radical-initiated organic aerosol oxidation. Journal of Physical Chemistry A 110, 3567–3577. doi:10.1021/jp0582383.

Farmer, D.K., Matsunaga, A., Docherty, K.S., Surratt, J.D., Seinfeld, J.H., Ziemann, P.J., Jimenez, J.L., 2010. Response of the Aerosol Mass Spectrometer to organonitrates and organosulfates and implications for field studies. Proceedings of the National Academy of Sciences of the United States of America, doi: 10.1073/pnas.0912340107.

Fry, J.L., Kiendler-Scharr, A., Rollins, A.W., Wooldridge, P.J., Brown, S.S., Fuchs, H., Dube, W., Mensah, A., dal Maso, M., Tillmann, R., Dorn, H.-P., Brauers, T., Cohen, R.C., 2009. Organic nitrate and secondary organic aerosol yield from NO_3 oxidation of beta-pinene evaluated using a gas-phase kinetics/aerosol partitioning model. Atmospheric Chemistry and Physics 9, 1431–1449.

Garnes, L.A., Allen, D.T., 2002. Size distributions of organonitrates in ambient aerosol collected in Houston, Texas. Aerosol Science and Technology 36, 983–992. doi:10.1080/02786820290092186.

Gilardoni, S., Russell, L.M., Sorooshian, A., Flagan, R.C., Seinfeld, J.H., Bates, T.S., Quinn, P.K., Allan, J.D., Williams, B., Goldstein, A.H., Onasch, T.B., Worsnop, D.R., 2007. Regional variation of organic functional groups in aerosol particles on four US east coast platforms during the International Consortium for Atmospheric Research on Transport and Transformation 2004 campaign. Journal of Geophysical Research – Atmospheres 112, D10S27. doi:10.1029/2006JD007737.

Gong, H.M., Matsunaga, A., Ziemann, P.J., 2005. Products and mechanism of secondary organic aerosol formation from reactions of linear alkenes with NO_3 radicals. Journal of Physical Chemistry A 109, 4312–4324. doi:10.1021/jo0580241.

Grover, B.D., Eatough, N.L., Woolwine, W.R., Cannon, J.P., Eatough, D.J., Long, R.W., 2008. Semi-continuous mass closure of the major components of fine particulate matter in Riverside, CA. Atmospheric Environment 42, 250–260. doi:10.1016/j.atmosenv.2007.09.037.

Hawkins, L.N., Russell, L.M., Quinn, P.K., Bates, T.S., Covert, D.S. Carboxylic acids, sulfates, and organosulfates in processed continental organic aerosol over the Southeast Pacific Ocean during VOCALS-REx 2008. Journal of Geophysical Research – Atmospheres, in press, doi:10.1029/2009JD013276.

Hopke, P.K., Barrie, L.A., Li, S.M., Cheng, M.D., Li, C., Xie, Y., 1995. Possible sources and preferred pathways for biogenic and non-sea-salt sulfur for the high arctic. Journal of Geophysical Research – Atmospheres 100, 16595–16603.

Jayne, J.T., Leard, D.C., Zhang, X., Davidovits, P., Smith, K.A., Kolb, C.E., Worsnop, D.R., 2000. Development of an Aerosol Mass Spectrometer for size and composition analysis of submicron particles. Aerosol Science and Technology 33, 49–70.

Jimenez, J.L., Jayne, J.T., Shi, Q., Kolb, C.E., Worsnop, D.R., Yourshaw, I., Seinfeld, J.H., Flagan, R.C., Zhang, X., Smith, K.A., Morris, J.W., Davidovits, P., 2003. Ambient aerosol sampling using the Aerodyne Aerosol Mass Spectrometer. Journal of Geophysical Research 108 (D7), 8425. doi:10.1029/2001JD001213.

Laurent, J.P., Allen, D.T., 2004. Size distributions of organic functional groups in ambient aerosol collected in Houston, Texas. Aerosol Science and Technology 38, 82–91. doi:10.1080/02786820390229561.

Lim, Y.B., Ziemann, P.J., 2009. Chemistry of secondary organic aerosol formation from OH radical-initiated reactions of linear, branched, and cyclic alkanes in the presence of NO_x. Aerosol Science and Technology 43, 604–619. doi:10.1080/02786820902802567.

Liu, S., Takahama, S., Russell, L.M., Gilardoni, S., Baumgardner, D., 2009. Oxygenated organic functional groups and their sources in single and submicron organic particles in MILAGRO 2006 campaign. Atmospheric Chemistry and Physics 9, 6849–6863.

Maria, S.F., Russell, L.M., Turpin, B.J., Porcja, R.J., 2002. FTIR measurements of functional groups and organic mass in aerosol samples over the Caribbean. Atmospheric Environment 36, 5185–5196.

Maria, S.F., Russell, L.M., Turpin, B.J., Porcja, R.J., Campos, T.L., Weber, R.J., Huebert, B.J., 2003. Source signatures of carbon monoxide and organic functional groups in Asian Pacific Regional Aerosol Characterization Experiment (ACE-Asia) submicron aerosol types. Journal of Geophysical Research – Atmospheres 108, 8637. doi:10.1029/2003JD003703.

Matsunaga, A., Ziemann, P.J., 2009. Yields of beta-hydroxynitrates and dihydroxynitrates in aerosol formed from OH radical-initiated reactions of linear alkenes in the presence of NO_x. Journal of Physical Chemistry A 113, 599–606. doi:10.1021/jp807764d.

Middlebrook, A.M., Matthew, B.M., Bahreini, R., Allan, J.D., Drewnick, F., Jimenez, J.L., Onasch, T.B., Canagaratna, M., Jayne, J.T., Worsnop, D.R. Fragmentation patterns and ionization efficiencies of oxygen, water, nitrate, sulfate, and ammonium with the Aerodyne Aerosol Mass Spectrometer. Aerosol Measurement Techniques, submitted for publication.

Mylonas, D.T., Allen, D.T., Ehrman, S.H., Pratsinis, S.E., 1991. The sources and size distributions of organonitrates in Los-Angeles aerosol. Atmospheric Environment Part A – General Topics 25, 2855–2861.

Ng, N.L., Kwan, A.J., Surratt, J.D., Chan, A.W.H., Chhabra, P.S., Sorooshian, A., Pye, H.O. T., Crounse, J.D., Wennberg, P.O., Flagan, R.C., Seinfeld, J.H., 2008. Secondary organic aerosol (SOA) formation from reaction of isoprene with nitrate radicals (NO_3). Atmospheric Chemistry and Physics 8, 4117–4140.

O'Brien, R.J., Crabtree, J.H., Holmes, J.R., Hoggan, M.C., Bockian, A.H., 1975. Formation of photochemical aerosol from hydrocarbons. Atmospheric analysis. Environmental Science & Technology 9, 577–582. doi:10.1021/es60104a004.

Quinn, P.K., Bates, T.S., Coffman, D., Onasch, T.B., Worsnop, D., Baynard, T., de Gouw, J.A., Goldan, P.D., Kuster, W.C., Williams, E., Roberts, J.M., Lerner, B., Stohl, A., Pettersson, A., Lovejoy, E.R., 2006. Impacts of sources and aging on submicrometer aerosol properties in the marine boundary layer across the Gulf of Maine. Journal of Geophysical Research – Atmospheres 111. doi:10.1029/2006jd007582.

Roberts, J.M., 1990. The atmospheric chemistry of organic nitrates. Atmospheric Environment Part A – General Topics 24, 243–287.

Russell, L.M., 2003. Aerosol organic-mass-to-organic-carbon ratio measurements. Environmental Science & Technology 37, 2982–2987. doi:10.1021/es026123w.

Russell, L.M., Takahama, S., Liu, S., Hawkins, L.N., Covert, D.S., Quinn, P.K., Bates, T.S., 2009. Oxygenated fraction and mass of organic aerosol from direct emission and atmospheric processing collected on the R/V Ronald Brown during TEX-AQS/GoMACCS 2006. Journal of Geophysical Research – Atmospheres 114. doi:10.1029/2008JD011275.

Russell, L.M., Hawkins, L., Frossard, A., Quinn, P.K., Bates, T.S. Carbohydrate-like composition of submicron atmospheric particles and their production from ocean bubble bursting. In: Proceedings of the National Academy of Sciences of the United States of America, in press, doi:10.1073/pnas.0908905107

Sage, A.M., Weitkamp, E.A., Robinson, A.L., Donahue, N.M., 2008. Evolving mass spectra of the oxidized component of organic aerosol: results from aerosol mass spectrometer analyses of aged diesel emissions. Atmospheric Chemistry and Physics 8, 1139–1152.

Sardar, S.B., Fine, P.M., Mayo, P.R., Sioutas, C., 2005. Size-fractionated measurements of ambient ultrafine particle chemical composition in Los Angeles using the NanoMOUDI. Environmental Science & Technology 39, 932–944. doi:10.1021/es049478j.

Sato, K., 2008. Detection of nitrooxypolyols in secondary organic aerosol formed from the photooxidation of conjugated dienes under high-NO_x conditions. Atmospheric Environment 42, 6851–6861. doi:10.1016/j.atmosenv.2008.05.010.

Seinfeld, J.H., Pandis, S.N., 2006. Atmospheric Chemistry and Physics, second ed. John Wiley & Sons, Inc., New York.

Ulbrich, I.M., Canagaratna, M.R., Zhang, Q., Worsnop, D.R., Jimenez, J.L., 2009. Interpretation of organic components from positive matrix factorization of aerosol mass spectrometric data. Atmospheric Chemistry and Physics 9, 2891–2918.

Zhang, Q., Alfarra, M.R., Worsnop, D.R., Allan, J.D., Coe, H., Canagaratna, M.R., Jimenez, J.L., 2005a. Deconvolution and quantification of hydrocarbon-like and oxygenated organic aerosols based on aerosol mass spectrometry. Environmental Science & Technology 39, 4938–4952. doi:10.1021/es048568I.

Zhang, Q., Worsnop, D.R., Canagaratna, M.R., Jimenez, J.L., 2005b. Hydrocarbon-like and oxygenated organic aerosols in Pittsburgh: insights into sources and processes of organic aerosols. Atmospheric Chemistry and Physics 5, 3289–3311.

Zhang, Q., Jimenez, J.L., Canagaratna, M.R., Allan, J.D., Coe, H., Ulbrich, I., Alfarra, M. R., Takami, A., Middlebrook, A.M., Sun, Y.L., Dzepina, K., Dunlea, E., Docherty, K., DeCarlo, P.F., Salcedo, D., Onasch, T., Jayne, J.T., Miyoshi, T., Shimono, A., Hatakeyama, S., Takegawa, N., Kondo, Y., Schneider, J., Drewnick, F., Borrmann, S., Weimer, S., Demerjian, K., Williams, P., Bower, K., Bahreini, R., Cottrell, L., Griffin, R.J., Rautiainen, J., Sun, J.Y., Zhang, Y.M., Worsnop, D.R., 2007. Ubiquity and dominance of oxygenated species in organic aerosols in anthropogenically-influenced Northern Hemisphere midlatitudes. Geophysical Research Letters 34, L13801. doi:10.1029/2007GL029979.

Zhang, X.F., Smith, K.A., Worsnop, D.R., Jimenez, J.L., Jayne, J.T., Kolb, C.E., Morris, J.W., Davidovits, P., 2004. Characterization of particle beam collimation. Part II: integrated aerodynamic lens-nozzle system. Aerosol Science and Technology 38, 619–638.